Phase shift of oscillatory magnetoresistance in a double-cross thin film structure of $La_{0.3}Pr_{0.4}Ca_{0.3}MnO_3$ via strain-engineered elongation of electronic domains

H. S. Alagoz,[1,*] B. Prasad,[2,3] J. Jeon,[1] M. G. Blamire,[2] K. H. Chow,[1,†] and J. Jung[1,‡]

[1]*Department of Physics, University of Alberta, Edmonton, Alberta, Canada T6G 2E1*

[2]*Department of Materials Science and Metallurgy, University of Cambridge, 27 Charles Babbage Road, Cambridge CB3 0FS, United Kingdom*

[3]*Department of Materials Science and Engineering, University of California Berkeley, Berkeley, California 94720, USA*

(Received 7 September 2017; revised manuscript received 26 December 2017; published 15 February 2018)

The subtle balance between the competing electronic phases in manganites due to complex interplay between spin, charge, and orbital degrees of freedom could allow one to modify the properties of electronically phase separated systems. In this paper, we show that the phase shift in the oscillatory magnetoresistance $\rho(\theta)$ can be modified by engineering strain driven elongation of electronic domains in $La_{0.3}Pr_{0.4}Ca_{0.3}MnO_3$ (LPCMO) thin films. Strain-driven elongation of magnetic domains can produce different percolation paths and hence different anisotropic magnetoresistance responses. This tunability provides a unique control that is unattainable in conventional 3*d* ferromagnetic metals and alloys.

DOI: 10.1103/PhysRevB.97.085129

I. INTRODUCTION

$(La_{1-x}Pr_x)_{1-y}Ca_yMnO_3$ (LPCMO) crystals and thin films are becoming prominent materials among transition-metal oxides because of their fascinating magnetic and electrical properties. Some examples are the supercooling glass transition in single-crystal $La_{0.225}Pr_{0.4}Ca_{0.375}MnO_3$ [1], giant discrete steps of resistivity near the metal-insulator transition (MIT) in spatially confined $La_{0.325}Pr_{0.3}Ca_{0.375}MnO_3$ films [2], and colossal magnetocapacitance (CMC) response in $(La_{0.5}Pr_{0.5})_{0.66}Ca_{0.33}MnO_3$ films [3]. Both theoretical and experimental studies have revealed the delicate balance between ferromagnetic metallic (FMM) and charge ordering insulating (COI) phases, suggesting that electronic phase separation (EPS) in LPCMO plays an important role in producing these interesting magnetotransport properties [4,5]. However, the physical origin of the EPS in LPCMO manganites is not fully understood partly because of the complex nature of these strongly correlated systems.

The EPS was also demonstrated to be an essential ingredient for anisotropic magnetoresistance, AMR [i.e., the dependence of the resistance on the angle, $\rho(\theta)$], between the directions of the magnetic field and the current [6]. In sharp contrast to ferromagnetic metals and alloys, the AMR in EPS manganites exhibits an unusual temperature dependence with a large maximum in the vicinity of the metal-insulator transition [7].

Recent Monte Carlo simulations show that highly anisotropic resistivities in manganites are associated with an imbalance in orbital populations driven by the anisotropic double exchange (ADE) and anisotropic Jahn-Teller (AJT) distortions [8]. These studies further suggest that ADE and AJT could reshape ferromagnetic clusters resulting in anisotropic percolation. Specifically, the Jahn-Teller interaction is weakened due to the bond angle of Mn-O-Mn being closer to 180° in the larger strain direction, whereas double exchange interaction remains unaffected due to the negligible bond length change. Such anisotropic modification of the JT and DE interactions could therefore lead to anisotropic FMM clusters. The nucleated FMM regions are electrically connected and hence promote easier percolation in one crystallographic direction than in the other. Unfortunately, little attention was paid to study the role of the strain driven shape of electronic domains on the AMR phenomena. Specifically, comprehensive observations are needed to understand the underlying correlations between the shape of the elongated ferromagnetic domains and AMR in strongly correlated systems.

In this paper, we present angular dependent resistivity measurements in the EPS sensitive thin films in which current directions are locked to certain lattice directions. This was done in order to learn about the behavior of the elongated domain rotation and its effect on the magnetotransport properties of these materials. Specifically, we would like to answer the following questions: (1) What is the oscillatory magnetoresistance $\rho(\theta)$ measured along various directions of percolation channels in the EPS system? (2) How does the type of elastic strain (isotropic and uniaxial) influence the shape of the electronic domains and the resultant $\rho(\theta)$? The answer to these questions would help one to understand the microscopic origin of the AMR and to tune its values. This would be useful for fabrication of technologically promising devices, such as magnetic random access memory (MRAM) and AMR based magnetic devices.

II. EXPERIMENTAL DETAILS

In order to study the role of elastic strain on the relationship between domain elongation and AMR, we designed

*alagoz@ualberta.ca
†khchow@ualberta.ca
‡jjung@ualberta.ca

experiments that allowed us to perform $\rho(\theta)$ measurements in four crossbarlike patterned $La_{0.3}Pr_{0.4}Ca_{0.3}MnO_3$ thin films grown on (100)- and (001)-oriented orthorhombic $NdGaO_3$ (NGO), and (001)-oriented cubic $(LaAlO_3)_{0.3}$-$(Sr_2AlTaO_6)_{0.7}$ substrates. These substrates produce epitaxial lattice strain of different magnitudes, anisotropy, and signs (compressive/tensile) in the plane of the LPCMO film. LSAT gives rise to isotropic tensile strain, whereas NGO(001) and NGO(100) produce uniaxial strains.

The 45-nm-thick LPCMO films were deposited, in an off-axis 50-W dc magnetron sputter deposition system, on atomically flat (i.e., ≈0.34 nm) scratch-free LSAT and NGO substrates at a temperature of 750 °C. These films were grown in an argon-oxygen mixture of partial argon and oxygen pressures of 20 and 100 mTorr, respectively. After the deposition, the chamber was filled with oxygen at atmospheric pressure in order to ensure the optimum oxygen content in these samples. The films were then *in situ* cooled down to 650 °C with a rate of 10 °C/min, followed by annealing at 650 °C for 3 h and subsequent cooling to room temperature with a rate of about 15 °C/min. LPCMO thin film patterns which consist of four 0.5-mm-wide and 5-mm-long bars, with an angle of 45° between adjacent bars, have been fabricated using conventional optical lithography [see Fig. 1(a)]. A chemical solution of HCI + H_2O + KI was used for the wet etching at a rate of 0.6 nm/s. On each bar, four silver pads, two serving as current and two as voltage contacts, were sputter deposited with the aid of a metal shadow mask. The prepatterned films on LSAT and NGO(100) exhibit clear Laue fringes in the x-ray diffraction (XRD) scan showing smooth surfaces and sharp interfaces with good uniformity, whereas Laue fringes for film on NGO(001) are not as coherent as those on other substrates [see the insets of Figs. 1(b)–1(d)].

The resistance R and its dependence on temperature, magnetic field, and the angle θ between the directions of the magnetic field **H** and the current **I** were measured with the standard four-point probe technique over a temperature range between 10 and 300 K, and in magnetic fields up to 1.1 T in the plane of the film. The motorized rotating drive (GMW 3473-MRD) was used to rotate the magnet from 0° to 180° while resistance and angle were collected simultaneously using LabVIEW drivers.

All magnetotransport measurements were carried out during the cooling cycle. In this case, $R(T)$ was collected when the sample was cooling in a 1.1-T magnetic field from 300 to 10 K. The measurements of $\rho(\boldsymbol{\theta})$ were performed using the following procedure: At 300 K, a maximum magnetic field **H** of magnitude 1.1 T was applied in the plane of the film at a certain angle θ relative to the direction of the current **I**. Then the sample's temperature was decreased until it reached the temperature of the measurement. The measurement of $\rho(\theta)$ was performed at a constant magnetic field by repetitive back and forth sweeping of θ between 0° and 180°. Due to the metastable irreversible state that exists in LPCMO films, resistivity decreases sharply with an increasing angle θ, and initially all films do not show expected oscillatory behavior. Regular symmetric oscillatory $\rho(\theta)$ behavior is observed after the sixth sweep of magnetic field. This is because magnetic field applied in a particular direction parallel to the film plane

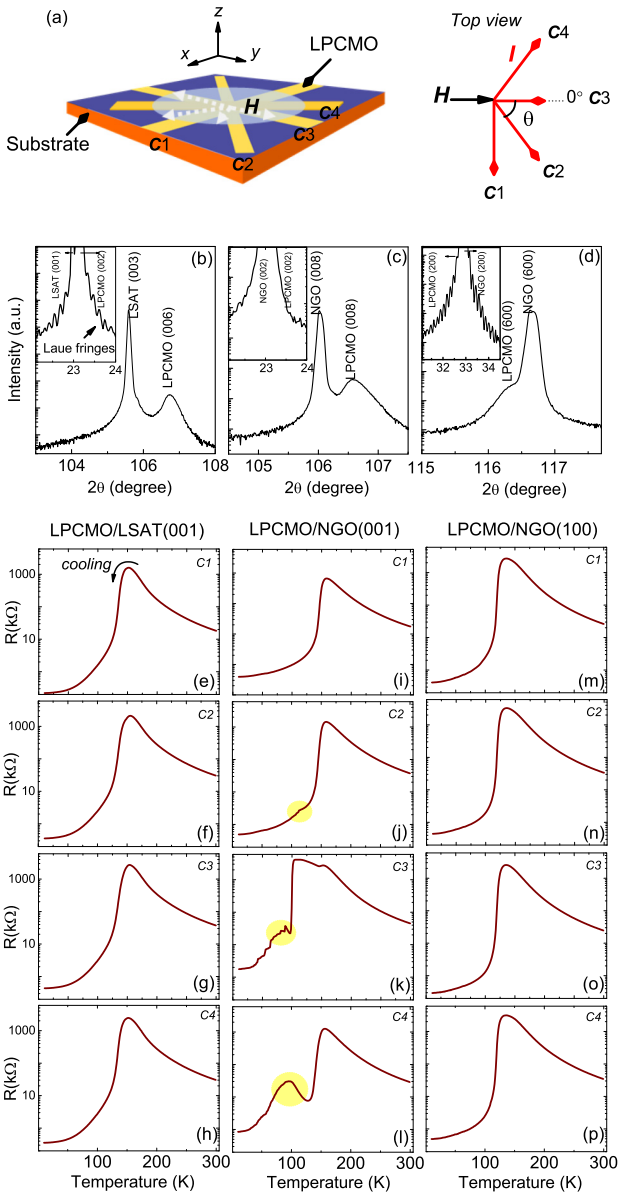

FIG. 1. (a) Schematics of the LPCMO four crossbar structure. The film is patterned into four bars; C_1, C_2, C_3, and C_4. Magnetic field **H** is applied and rotated in the xy plane of the film. Directions of the transport current (**I**) of 1 μA are indicated for each bar on the top view. (b)–(d) Intensity-2θ scans of LPCMO films deposited on LSAT(001), NGO(001), and NGO(100). Field-cooled R-T curves collected at $\theta = 0°$ (i.e., **H** parallel to current direction in C_3 only) and under 1.1-T field for all bars patterned on LSAT(001) (e)–(h), on NGO(001) (i)–(l), on NGO(100) (m)–(p) substrates, respectively. Phase instability (see the text) is detected at low temperatures for C_2, C_3, and C_4 bars on NGO(001).

causes a preferential expansion of the volume of FMM domains in that field direction. Hence, during the first angular sweep, by a continuous sweeping of the magnetic field direction in the film plane, the overall volume of FMM domains is increased dramatically. This leads to an enhanced percolation within the film and a dramatic drop of the resistivity to its "oscillatory" level [9].

III. RESULTS

Field-cooled $R(T)$ measurements collected for each section of the crossbars fabricated on LSAT(001), NGO(001), and NGO(100) are shown in Figs. 1(e)–1(p). The LPCMO crossbars deposited on LSAT, NGO(001), and NGO(100) show the metal-insulator transition temperatures (T_{MIT}) at 152, 159, and 135 K respectively. All bars patterned on LSAT and NGO(100) show metallic behavior with $d\rho/dT > 0$ far below their T_{MIT} values. However, a secondary T_{MIT} was observed for C_3 and C_4 patterned on NGO(001) surprisingly similar to that observed in spatially confined 10-μm $La_{0.325}Pr_{0.3}Ca_{0.375}MnO_3$ wire [10]. Secondary T_{MIT} in LPCMO/NGO(001) could be due to anisotropic strain relaxation which induces the inhomogeneity, thus enhancing phase instability in this film [11].

Examples of the dependence of the normalized resistivity (ρ/ρ_{max}) on the angle θ collected under 1.1-T magnetic fields for crossbars patterned on LSAT(001), NGO(001), and NGO(100) are shown in Figs. 2(a)–2(c). These measurements were carried out near the samples' metal-insulator transition temperatures. For films on LSAT, the maximum resistivity state (MRS) occurs at 90° for all bars [see Fig. 2(a)]. In the case of films on NGO(001) however, the MRS occurs at 0°, 45°, 90°, and 135° for the bars C_1, C_2, C_3, and C_4 respectively [see Fig. 2(b)]. Finally, Fig. 2(c) shows that the MRS state occurs at −90°, −45°, 0°, and 45° for the bars C_1, C_2, C_3, and C_4 respectively patterned on NGO(100) substrate.

Note that some of the bars exhibit a possible "phase shift" as the temperature is varied. This is illustrated by the plots in Figs. 3(a)–3(c), which shows the temperature dependence of the phase angles at which the maximum resistivity occurs for the C_1, C_2, C_3, and C_4 bars. The plots show the temperatures between 80 and 180 K where the $\rho(\theta)$ signals exhibit well-defined oscillatory shapes. The bars patterned on LSAT show the MRS state occurs at $\theta = 90°$ at all temperatures. By contrast, in the case of bars on NGO(001), the angle at which the MRS occurs changes with temperature. Specifically, the angles for C_1, C_3, and C_4 increase near the bars' metal-to-insulator temperatures. In the case of bars on NGO(100), the angles at which the MRS occur are clearly temperature independent for a particular bar. In particular the MRS state for C_1, C_2, C_3, and C_4 occurs at $\theta = 90°$, $\theta = -45°$, $\theta = 45°$, and $\theta = 0°$, respectively.

The $\rho(\theta)$ measurements presented in Figs. 2(a)–2(c) normally allow one to determine the in-plane AMR and its dependence on temperature for bars grown on LSAT, NGO(001), and NGO(100) substrates [see Figs. 3(a)–3(c)] using the well-known definition $[(\rho_\parallel - \rho_\perp)/(\rho_\parallel/3 + 2\rho_\perp/3)] \times 100\%$ where $\rho_\perp$ is the resistivity measured in a field of 1.1 T perpendicular to the current direction (i.e., ρ at $\theta = 90°$) and $\rho_\parallel$ is the resistivity measured with 1.1 T parallel to the current direction (i.e., ρ at $\theta = 0°$) [12]. However, since the extrema in the resistivity do not necessarily occur at $\theta = 0°$ and 90° for bars patterned on NGO substrates, we instead present Figs. 3(d)–3(f) in order to track the temperature dependence of the magnitude of the anisotropic magnetoresistance for the bars grown on LSAT, NGO(001), and NGO(100) substrates. In these three figures, the ordinate scales show the normalized difference between the maximum and minimum resistivity, $\Delta\rho = |[(\rho_{max} - \rho_{min})/\rho_{max}]|\%$, regardless of what

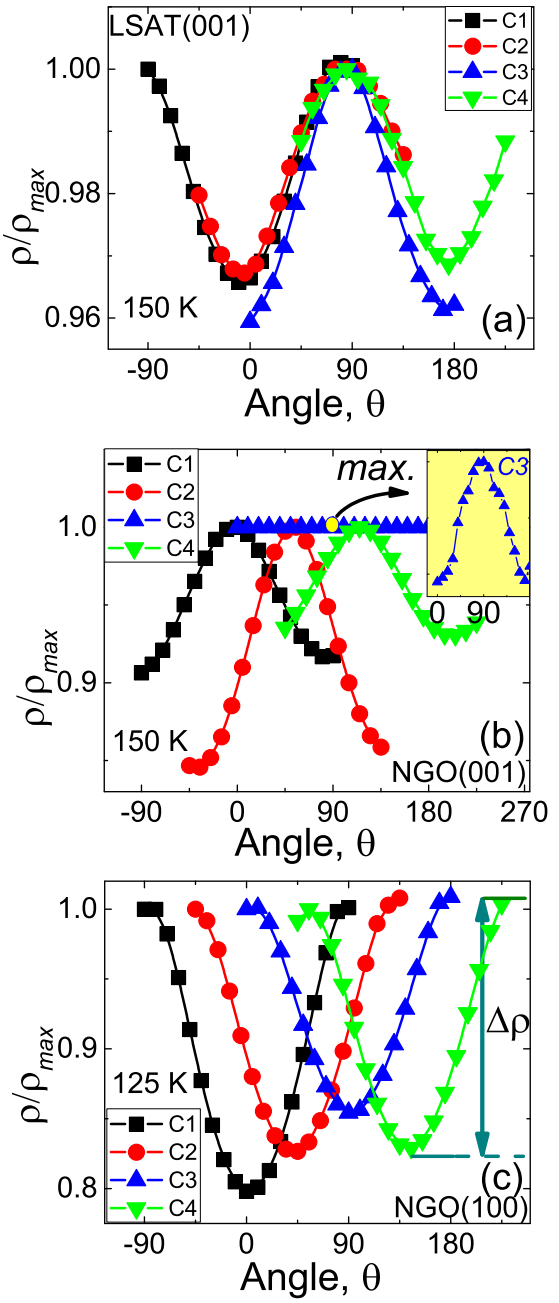

FIG. 2. (a)–(c) The dependence of the normalized resistivity on angle θ under 1.1 T measured for LPCMO crossbars patterned on LSAT(001), NGO(001), and NGO(100) substrates near the metal-insulator transition temperatures. The difference between maximum and minimum resistivity state is indicated as $\Delta\rho$ shown in (c).

angles these occur at. The maximum value of $\Delta\rho$ increases from LSAT (∼4%) to NGO(001) (∼10%) and to NGO(100) (∼20%) bars. Bars on LSAT and NGO(100) substrates show similar temperature behaviors (i.e., all show maxima in the temperature dependence of $\Delta\rho$ near their T_{MIT} values). On the other hand, certain bars such as C_2, C_3, and C_4 on NGO (001) substrate not only show peaks near their T_{MIT} values but also secondary peaks at lower temperatures.

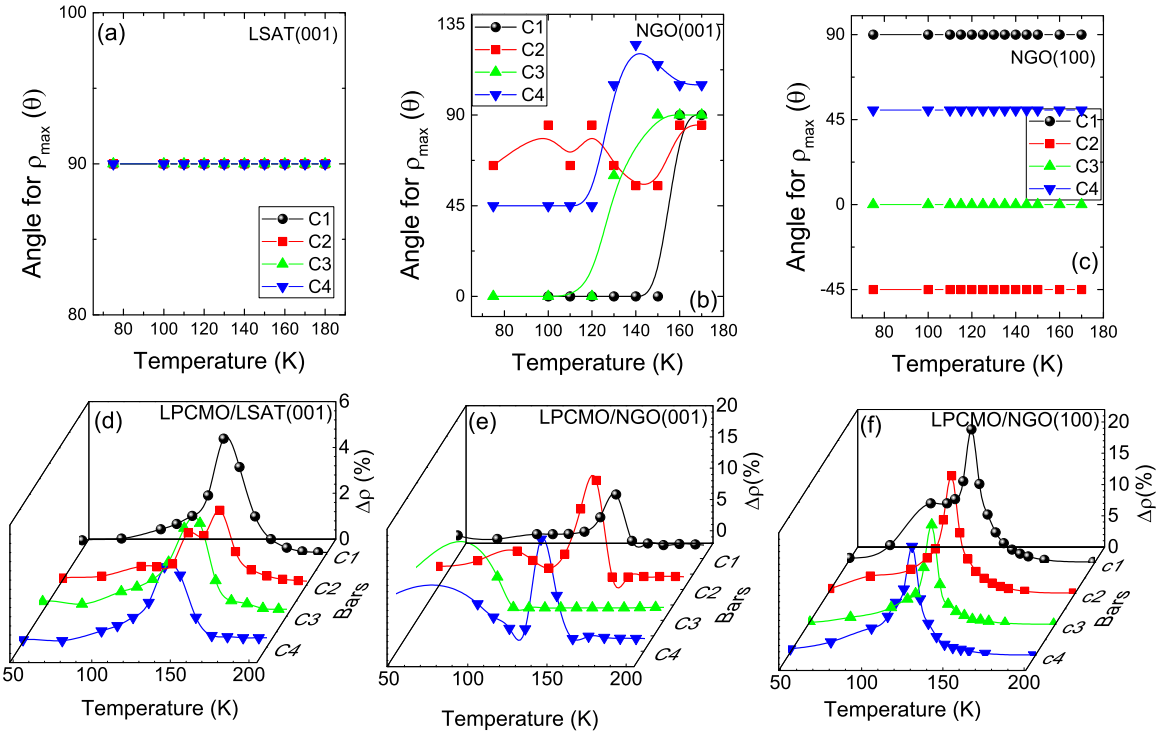

FIG. 3. (a)–(c) Temperature dependence of phase angle for maximum resistivity measured for bars patterned on LSAT, NGO(001), and NGO(100) substrates. (d)–(f) Magnitude of the difference between maximum and minimum resistivity, $\Delta\rho$ for LPCMO films patterned on LSAT(001), NGO(001), and NGO(100) substrates.

IV. DISCUSSION

What is the mechanism(s) of the gradual shift in the oscillatory magnetoresistance observed in bars patterned on NGO substrates? We believe that strain as well as magnetic field driven elongation of the FMM electronic domains within the percolation network play an important role in explaining our observations. It is believed that lower temperatures or higher magnetic fields cause the nucleation and growth of FMM domains in EPS materials, resulting in several percolating paths within the COI background/matrix [13,14]. What is the role of the isotropic and anisotropic strain on the percolative transport? Before addressing this question, we show in-plane Q maps and calculated strain values in Figs. 4(a) and 4(b). Substrates such as LSAT and NGO(001) have the same $Q_{\text{in-plane}}$ with the films indicating that coherent growth with identical in-plane lattice spacing takes place between the film and the substrate. On the other hand, the film on NGO (100) substrate have the same $Q_{\text{in-plane}}$ and $Q_{\text{out-of-plane}}$ indicating that the film and the substrate have same in-plane and out-of-plane lattice parameters. LPCMO films deposited on LSAT experience tensile strain along (100) and (010) directions with a value of $\varepsilon_a = +0.339$ and $\varepsilon_b = +0.382$, respectively. However, LPCMO film on NGO(001) experiences a tensile strain along (010) with $\varepsilon_b = +0.758$ and compressive along (100) directions with a strain value of $\varepsilon_a = -0.868$. LPCMO films on NGO(100) have tensile strain along (010) and (001) directions with strain values of $\varepsilon_b = +1.107$ and $\varepsilon_c = +0.337$. These results clearly indicate that the strain state of LPCMO on LSAT is nearly isotropic while the strain state for films on NGO(001) and NGO(100) is anisotropic.

Uniaxial strain could contribute to the shift in $\rho(\theta)$ observed for films deposited on NGO substrates. In the theoretical study by Dong *et al.*, anisotropic double exchange and Jahn-Teller distortions were shown to be responsible for the anisotropic transport in strained manganites [8]. Based on this theory, anisotropic strain causes a stronger overlap of the Mn orbitals along one crystallographic direction which

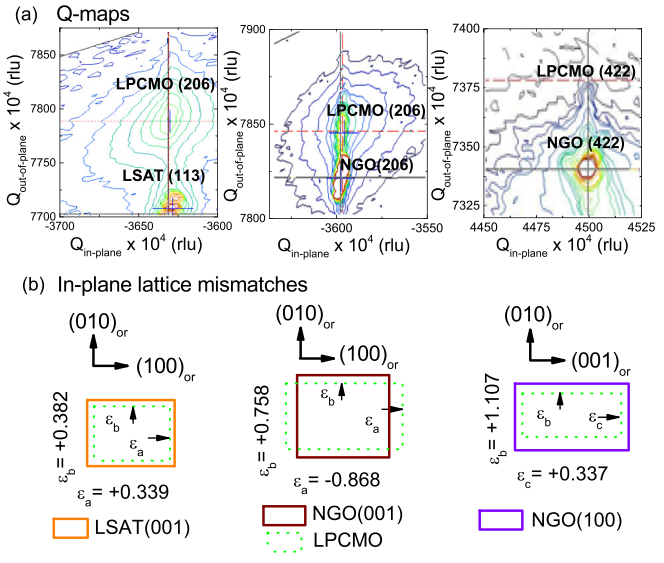

FIG. 4. (a) Reciprocal space maps of the (206) and (422) XRD reflections of a 45-nm LPCMO film on LSAT(001), NGO(001), and NGO(100), respectively. (b) Corresponding in-plane lattice mismatches between the film and substrates.

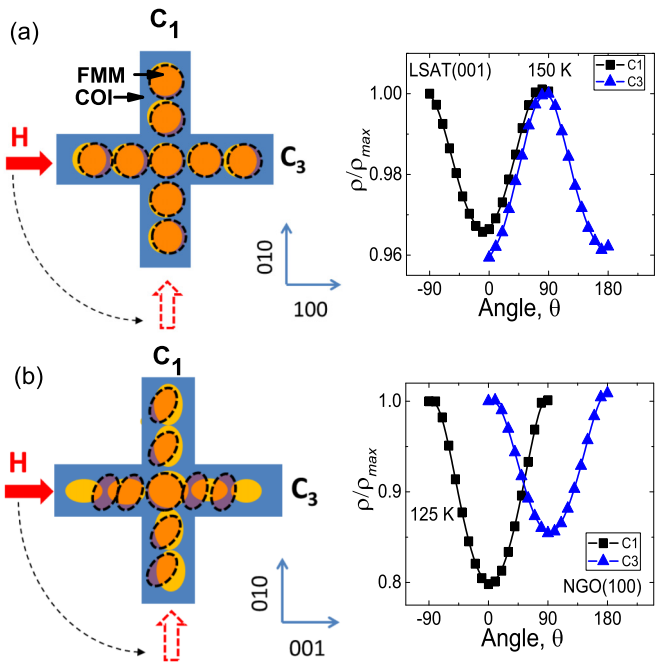

FIG. 5. Rotation of metallic domains (marked by dashed circles and ellipses) for C_1 and C_3 bars during the rotation of magnetic field from 0° (field parallel to current direction in C_3) to 90° (field parallel to current direction in C_1). Yellow and orange colored domains represent the orientation/distribution of these domains at 0° (solid arrow) to 90° (dashed arrow), respectively. (a) Domain elongation is negligible for isotropically strained LPCMO bars on LSAT resulting in zero shift in $\rho(\theta)$. (b) Domains are elongated due to uniaxial strain in LPCMO bars on NGO(100) causing anisotropic percolation channels and phase shift in $\rho(\theta)$.

makes conductivity more preferable along one crystallographic direction than along the other directions within the film. Similar arguments have been proposed for $Pr_{0.65}(Ca_{0.7}Sr_{0.3})MnO_3$ thin films deposited on (110)-oriented NGO substrates [15]. The anisotropy of the percolation path is enhanced when the aspect ratio of elongated metallic domains is increased by long-range elastic strain fields and applied magnetic fields [16,17].

In Figs. 5(a) and 5(b), we schematically show the FMM domain elongation/distribution of C_1 and C_3 bars patterned on LSAT(001) and NGO(100) substrates. According to this schematic, FMM domains are uniaxially elongated in the NGO substrate as compared to the film on LSAT where domains are not elongated. The yellow and orange colored domains in these schematics represent the orientation/distribution of these domains at magnetic fields applied parallel to the current direction in the C_1 and C_3 bars, respectively.

Consider first bars on LSAT [see Fig. 5(a)]; the magnetic field is at $\theta = 0°$ (field is applied parallel to current direction in C_3 but it is perpendicular to current direction in C_1), percolation easily takes place (i.e., yellow domains are connected) for both C_1 and C_3 and hence they are both in the low resistance state at this angle. When the magnetic field is at $\theta = 90°$ (field is applied parallel to current direction in C_1 but it is perpendicular to current direction in C_3), the domains are separated (orange colored domains are separated) and the bars C_1 and C_3 are in their maximum resistance states. The angular dependence of the domain rotation is expected to be similar for both bars due to isotropic strain resulting in the absence of a shift in $\rho(\theta)$.

In the case of LPCMO/NGO(100) however, the percolation channel is anisotropic. This is schematically shown in Fig. 5(b). When field is applied parallel to the C_3 bar, we assume that domains are not connected for C_3 but percolation was already taken place for the C_1 bar. This could be due to a higher strain field present in C_1 ($\varepsilon_b = +1.107$) than in C_3 ($\varepsilon_c = +0.337$) which could produce easier percolation of domains in C_1 [16]. This can be seen in the $\rho(\theta)$ plot, where maximum and minimum resistance states occur for C_3 and C_1, respectively. When the field is applied parallel to the current direction in C_1, rotation of domains (see the dashed ellipses) in C_3 bars moves metallic domains closer, enhancing percolation. Therefore, the low resistance state is achieved for the C_3 bar. On the other hand, metallic domains are separated for C_1 during the rotation of magnetic field, resulting in a high resistance state. This proposed mechanism also applies to LPCMO/NGO(001) bars, where percolation and depercolation take place at an angle 90° shifted with respect to that for LPCMO/NGO(100) bars. The shift could be due to different sign arrangements of strain (i.e., compressive along a, tensile along b) present in LCPMO films grown on NGO(001). It has been shown that the sign of strain could affect the direction of easy axis magnetization and could cause a 90° shift in $\rho(\theta)$ in manganite films [18,19].

Here, it is worth mentioning strong variations of the phase angle [see Fig. 3(b)] on temperature observed for LCPMO bars fabricated on NGO(001) substrate. Interestingly, $R(T)$ measurements of these bars show a hump or secondary T_{MIT} which increases from the C_1 to C_4 bar at low temperatures. Furthermore, our field-warming (FW) and field-cooling (FC) resistance measurements show a large thermal hysteresis in these bars. All of these indications signify that bars on NGO(001) possess strong phase instability [20,21]. Strong phase instability along with possible chemical inhomogeneity could add further complexity by influencing the percolation path for the transport current and hence producing temperature variations in the phase angle. In order to disentangle magnetic and structural effects on the strong phase angle instability observed for LPCMO bars on NGO(001), we conducted transport measurements [i.e., $R(T)$], without applying an external magnetic field. The results indicate that bars show a hump or secondary T_{MIT} under zero magnetic field, indicating that the origin of the secondary T_{MIT} could stem from the structural effects rather than magnetic. The less coherent Laue fringes obtained for film on NGO(001) further confirms that observed secondary T_{MIT} in these films are of structural origin. It is also worth noting that the anisotropic strain driven structural defects in phase separated films could enhance insulating state at low temperatures, observed for manganite films deposited on NGO(001) substrates [22]. This explains the existence of secondary T_{MIT} in LPCMO films on NGO(001) and the non-systematic shift in the oscillatory dependence on temperature for these films.

Our proposed mechanism for the strain driven phase shift in the oscillatory magnetoresistance has been further tested for LPCMO crossbars patterned on $SrTiO_3$ (STO), $LaAlO_3$ (LAO), and NGO(001) substrates. In these samples, C_4 and C_2

bars form an angle of 27° (instead of 45°) with C_1. LPCMO bars on cubic STO and LAO substrates show no phase shift in $\rho(\theta)$. However, bars of LPCMO/NGO(001) show a phase shift in $\rho(\theta)$ measured from C_1 to C_4 bars. Collectively, these results demonstrate that the phase shifts in the oscillatory magnetoresistance are not simply due to the angle that the bars form with each other, but rather on the presence of anisotropic strain due to the noncubic nature of the substrate.

V. CONCLUSION

We have found that uniaxially strained LPCMO films show large phase shifts in their oscillatory magnetoresistance whereas films deposited on cubic substrates show no shift in their oscillatory magnetoresistance. These results imply that long-range uniaxial strain field along with magnetic field elongate the metallic domains resulting in different percolative channels and hence the observed phase shifts. These results provide useful information that allows one to understand electronic domain dynamics and its direct effect on the oscillatory magnetoresistive properties of strained manganites at the microscopic level.

ACKNOWLEDGMENT

This work was partially supported by the Natural Sciences and Engineering Research Council of Canada.

[1] W. Wu, C. Israel, N. Hur, S. Park, S.-W. Cheong, and A. DeLozanne, Nat. Mater. **5**, 881 (2006).
[2] H. Y. Zhai, J. X. Ma, D. T. Gillaspie, X. G. Zhang, T. Z. Ward, E. W. Plummer, and J. Shen, Phys. Rev. Lett. **97**, 167201 (2006).
[3] R. P. Rairigh, G. Singh-Bhalla, S. Tongay, T. Dhakal, A. Biswas, and A. F. Hebard, Nat. Phys. **3**, 551 (2007).
[4] M. Uehara, S. Mori, C. H. Shen, and S.-W. Cheong, Nature (London) **399**, 560 (1999).
[5] A. Moreo, S. Yunoki, and E. Dagotto, Science **283**, 2034 (1999).
[6] H. S. Alagoz, M. Khan, M. M. Saber, S. T. Mahmud, K. H. Chow, and J. Jung, Appl. Phys. Lett. **102**, 242406 (2013); H. S. Alagoz, J. Jeon, R. Boos, R. H. Ahangharnejhad, K. H. Chow, and J. Jung, *ibid.* **105**, 162409 (2014).
[7] M. Egilmez, K. H. Chow, and J. Jung, Mod. Phys. Lett. B **25**, 697 (2011).
[8] S. Dong, S. Yunoki, X. Zhang, C. Sen, J. M. Liu, and E. Dagotto, Phys. Rev. B **82**, 035118 (2010).
[9] H. S. Alagoz, J. Jeon, S. T. Mahmud, M. M. Saber, B. Prasad, M. Egilmez, K. H. Chow, and J. Jung, Appl. Phys. Lett. **103**, 232402 (2013).
[10] T. Z. Ward, S. Liang, K. Fuchigami, L. F. Yin, E. Dagotto, E. W. Plummer, and J. Shen, Phys. Rev. Lett. **100**, 247204 (2008).
[11] Z. Huang, G. Gao, Z. Yin, X. Feng, Y. Chen, X. Zhao, J. Sun, and W. Wu, J. Appl. Phys. **105**, 113919 (2009).
[12] T. R. McGuire and A. R. I. Potter, IEEE Trans. Magn. **MAG-11**, 1018 (1975).
[13] H. Jeen and A. Biswas, Phys. Rev. B **88**, 024415 (2013).
[14] T. Dhakal, J. Tosado, and A. Biswas, Phys. Rev. B **75**, 092404 (2007).
[15] C. L. Lu, Y. Y. Wu, Z. C. Xia, S. L. Yuan, L. Chen, Z. M. Tian, J.-M. Liu, and T. Wu, Appl. Phys. Lett. **99**, 122510 (2011).
[16] T. Z. Ward, J. D. Budai, Z. Gai, J. Z. Tischler, L. Yin, and J. Shen, Nat. Phys. **5**, 885 (2009).
[17] G. Singh-Bhalla, A. Biswas, and A. F. Hebard, Phys. Rev. B **80**, 144410 (2009).
[18] H. S. Alagoz, J. Desomberg, M. Taheri, F. S. Razavi, K. H. Chow, and J. Jung, Appl. Phys. Lett. **106**, 082407 (2015).
[19] M. Egilmez, M. M. Saber, A. I. Mansour, R. C. Ma, K. H. Chow, and J. Jung, Appl. Phys. Lett. **93**, 182505 (2008).
[20] Z. Huang, L. F. Wang, X. L. Tan, P. F. Chen, G. Y. Gao, and W. B. Wu, J. Appl. Phys. **108**, 083912 (2010).
[21] F. H. Zhang, Z. Huang, G. Y. Gao, P. F. Chen, L. F. Wang, X. L. Tan, and W. B. Wu, Appl. Phys. Lett. **96**, 062507 (2010).
[22] B. W. Zhi, G. Y. Gao, Z. Huang, L. F. Wang, X. L. Tan, P. F. Chen, and W. B. Wu, J. Appl. Phys. **113**, 203701 (2013).